# Connectivity-Altering Monte Carlo Simulations of the End Group Effects on Volumetric Properties for Poly(ethylene oxide)

**Collin D. Wick and Doros N. Theodorou***

*School of Chemical Engineering, Department of Materials Science and Engineering, National Technical University of Athens, 9 Heroon Polytechniou Street, Zografou Campus, 15780 Athens, Greece*

*Received April 26, 2004; Revised Manuscript Received June 21, 2004*

ABSTRACT: Connectivity-altering Monte Carlo simulations have been used to study structure−property relationships of poly(ethylene glycol) (PEG) and poly(ethylene oxide) dimethyl ether (PEODME) using the recently developed transferable potentials for phase equilibria united atom (TraPPE-UA) ether and alkanol force fields. The combination of end-bridging and double-bridging Monte Carlo simulation techniques is shown to do a good job of equilibrating moderate to high molecular weight polymer melts. Results give excellent agreement between experiment and simulation for liquid densities at a variety of temperatures, pressures, and molecular weights. Comparisons are also made with experiment for structural properties, including the structure factor, chain mean squared end-to-end distance, and radius of gyration, showing good agreement with experiment. Moreover, a thorough microscopic analysis is performed on the different end group effects of PEG and PEODME, determining the excluded volume and liquid structure around the end groups, and linking these to their volumetric properties.

## Introduction

Poly(ethylene oxide) (PEO) alone, or as part of copolymers has a variety of technologically important uses, including drug delivery,[1] protein partitioning,[2] polymer surfactants,[3,4] and polymer electrolytes.[5−8] Because of the importance of PEO, a large number of experimental and theoretical investigations of its structure−property relationships have been undertaken.[9−13] A majority of the theoretical studies consist of molecular dynamics (MD) simulations of PEODME polymers of low to moderate molecular weight. Many applications, however, call for high molecular weight PEO, which cannot be reliably equilibrated with MD methods in a reasonable amount of computer time. This can be brought to light by realizing that the longest relaxation time of an entangled polymer melt of length $n$ scales at least as $n^3$.[14] With the development of connectivity-altering Monte Carlo methods,[15−17] though, it is now possible to equilibrate high molecular weight polymers by reconnecting inner polymer segments, which makes equilibration nearly independent of chain length.

PEO is usually end-capped by either methyl or alkanol groups, and the type of end group has been shown to have a significant effect on its volumetric properties. For instance, while methyl capped PEO exhibits a moderate increase in density with increasing degree of polymerization, the density of alkanol capped PEO varies very little with molecular weight.[18,19] It has been conjectured that the origin of this discrepancy is the different molar volumes of the end groups, and lower degrees of freedom for the alkanol end group.[18] This was made with the use of equation-of-state theories from Flory and co-workers,[20] and Lennard-Jones and Devonshire,[21] but without a reliable microscopic picture to base their conclusions. Molecular simulation is an excellent tool for lending microscopic insight into macroscopic observables, and in particular for probing the microscopic origins of the end-capping effects on PEO structure and volumetric properties.

* Corresponding author: doros@central.ntua.gr

Quality all-atom force fields exist for PEO, which can reproduce structural and thermodynamic properties over varying ranges of conditions.[12,22−24] The transferable potentials for phase equilibria united atom (TraPPE-UA) force field can be an attractive alternative to these in certain situations, since it reduces the number of interaction sites required by treating methyl, methylene, and methine groups as single sites, yet it has been shown to do very well in reproducing pure and multiphase thermodynamic properties.[25−29] For certain applications, for instance studying dynamics of ion transport through PEO with nanoparticle fillers,[7] a more complicated force field may be required. Nevertheless, a united atom model could still be useful for these applications; equilibration of the long-ranged explicit order of the polymer, with such a model, could be followed by mapping onto a more complex (and computationally more expensive) atomistic model for local equilibration and dynamics study.

While the TraPPE-UA force field has been shown to be good for simulating small to moderately sized molecules, it has not been tested for molecules with high molecular weights. Here, the TraPPE-UA ether, alkanol, and glycol force fields,[28,29] which were fit to reproduce the vapor−liquid coexistence properties of small molecules, are used to predict volumetric and structural properties of medium to high molecular weight PEG and PEODME polymers with connectivity-altering Monte Carlo algorithms. The efficiencies of the different Monte Carlo algorithms are tested and compared, along with assessing the reproducibility of experimental volumetric properties at varying molecular weights, temperatures, and pressures, to ensure that the force field is robust. In addition, conformational and structural properties are compared with both experiment and previously developed force fields. Finally, after the validation of the force field and simulation methods, a microscopic analysis of the end group effect on volumetric and structural properties is undertaken.

10.1021/ma049193r CCC: $27.50 
Published on Web 08/07/2004

**Table 1. Potential Parameters Used to Simulate PEG and PEODME**

| stretch | bond length (Å) | stretch | bond length (Å) |
|---|---|---|---|
| $CH_x$-O(ether) | 1.41 | H−O | 0.945 |
| $CH_x$-O(alkanol) | 1.43 | $CH_x$-$CH_x$ | 1.54 |

| bend (eq 1) | $k_\theta$ (K) | $\theta_0$ (deg) |
|---|---|---|
| $CH_x$-O−$CH_y$ | 30 200 | 112 |
| $CH_x$-$CH_2$−O (ether) | 25 150 | 112 |
| $CH_x$-$CH_2$−O (alkanol) | 17 640 | 109.5 |
| H−O−$CH_x$ | 27 720 | 108.5 |

| torsion (eq 2) | $c_1$ (K) | $c_2$ (K) | $c_3$ (K) |
|---|---|---|---|
| $CH_x$-O−$CH_2$−$CH_2$ | 725.35 | 163.75 | 558.2 |
| H−O−$CH_2$−$CH_2$ | 209.82 | −29.17 | 187.93 |

| torsion (eq 3) | $c_1$ (K) | $c_2$ (K) |
|---|---|---|
| O−$CH_2$−$CH_2$−O | 475 | 475 |

| nonbond (eq 3) | $\sigma$ (Å) | $\epsilon$ (K) | $q$ |
|---|---|---|---|
| $CH_3$ | 3.75 | 98 | 0.25 |
| $CH_2$ (ether) | 3.95 | 46 | 0.25 |
| $CH_2$ (alkanol) | 3.95 | 46 | 0.265 |
| O (ether) | 2.85 | 55 | −0.5 |
| O (alkanol) | 3.02 | 93 | −0.7 |
| H | 0 | 0 | 0.435 |

## Molecular Model

The TraPPE-UA force field utilizes pseudo-atoms for methyl and methylene groups located at the carbon centers, and models all oxygens and hydroxy hydrogens explicitly.[25−29] Polymer chains are treated as semiflexible with fixed bond lengths and flexible bond angles and dihedrals. Bond angles are governed by a harmonic bond bending potential.

$$u_{\text{bend}} = \frac{k_\theta}{2}(\theta - \theta_0)^2 \tag{1}$$

where $k_\theta$ and $\theta_0$ are the force constant and equilibrium bond angle respectively, and are given in Table 1. For all dihedral interactions except O−$CH_2$−$CH_2$−O, a cosine series of the familiar OPLS form[30] is used.

$$u_{\text{tors}} = c_1(1 + \cos(\phi)) + c_2(1 - \cos(2\phi)) + c_3(1 + \cos(3\phi)) \tag{2}$$

where the values for the $c_n$ constants are given in Table 1. For the O−$CH_2$−$CH_2$−O dihedral, a slightly modified potential is used, which was fit to reproduce the torsional distributions of the force field proposed by Smith and co-workers.[22]

$$u_{\text{tors}} = c_1[1 - \cos(\phi)] + c_2\left\{1 - \cos\left[2\left(\phi + \frac{\pi}{2}\right)\right]\right\} \tag{3}$$

where the $c_n$ constants are given in Table 1. The difference between the $c_2$ value used here and that used in ref 22 is discussed below. The pairwise nonbonded interaction potential for atoms $i$ and $j$, separated by a distance of $r_{ij}$, is a combination of Lennard-Jones (LJ) 12−6 and Coulombic potentials.

$$u_{\text{LJ}}(r_{ij}) = 4\epsilon_{ij}\left[\left(\frac{\sigma_{ij}}{r_{ij}}\right)^{12} - \left(\frac{\sigma_{ij}}{r_{ij}}\right)^{6}\right] \tag{4}$$

$$u_{\text{coul}} = S\frac{q_i q_j}{4\pi\epsilon_0 r_{ij}} \tag{5}$$

where $\sigma$, $\epsilon$, and $q_i$ are the LJ well depth, LJ diameter, and atomic charge respectively, and the values used here are given in Table 1. For all intermolecular interactions and intramolecular interactions between atoms separated by four or more bonds, $S$ is one, while for all intramolecular interactions between atoms separated by three bonds, $S$ is 0.5 and $u_{\text{LJ}}$ is zero. For unlike interactions, the standard Lorentz−Berthelot combining rules are used.[31,32] Unlike here, Smith and co-workers use full nonbonded interactions for atoms separated by three bonds,[22] creating the need to rescale the $c_2$ parameter in eq 3 to get the same torsional distribution in our case. The reasoning behind not including LJ interactions between atoms separated by three bonds is to avoid the very high repulsion that can result from such interactions, which in many cases alters the bond angles moderately from their equilibrium values (Smith and co-workers use a softer exponential-6 potential). As a consequence of the model implementation, a problem arises for special cases where intramolecular hydrogen bond donors and acceptors are separated by exactly four bonds, and specifically for glycol end groups (H−O−$CH_2$−$CH_2$−O). This is because there is no LJ site at the hydrogen atom, and the two oxygens do not repel each other since they are separated by three bonds. To remedy this, a repulsive potential between the hydrogen and first ether oxygen is used of the form $a(1/r)^{12}$ with $a = 1 \times 10^7$ Å$^{12}$ K$^{-1}$, which was optimized to reproduce the vapor−liquid equilibria of 1,2-ethanediol, 2-methoxyethan-1-ol, and 1,2-dimethoxyethane.[29] The LJ potential is truncated for site−site distances greater than 12 Å, with analytical tail corrections and Ewald summations used to account for long-ranged LJ and Coulombic interactions, respectively.

The nonbonded parameters for the TraPPE force field are fit to reproduce vapor−liquid coexistence curves, and in some cases, vapor−solid and binary phase behavior. Further information on the parametrization methodology, and the specifics for the alkanol and ether groups can be found in refs 28 and 29.

## Simulation Methods and Details

A combination of the end-bridging (EB)[15] and double-bridging (DB)[16] Monte Carlo methods were the primary means of equilibrating the polymer chains. These methods, individually, have been repeatedly studied and shown to successfully sample the configuration space of a variety of polymer melts,[33−35] but never has a combination of the two methods been used. The semi-grand-canonical constant pressure ensemble $NnPT\boldsymbol{\mu}^*$ was used, which keeps the number of chains ($N$), the number of mers ($n$), the temperature ($T$), and a profile of relative chemical potentials ($\boldsymbol{\mu}^*$) constant.[15] In addition to end-bridging and double-bridging moves, volume fluctuations, translational, rotational, configurational-bias Monte Carlo (CBMC),[36,37] self-adapting fixed-end point configurational-bias Monte Carlo (SAFE-CBMC),[38] and CBMC reptation (for PEODME only) moves were used. All polymer systems had polydisperse chains, with uniform number distributions of chain lengths in the interval $[\bar{X}(1 - \Delta), \bar{X}(1 + (\Delta)]$, where $\bar{X}$ is the mean chain length, and $\Delta$ is the half-width of the chain length distribution reduced by the number-averaged chain length. The number-averaged molecular weight and the polydispersity, along with the number of polymer chains ($N$) simulated

**Table 2. System Parameters Used**

| name | $N$ | $M_n$ (g/mol) | $M_w/M_n$ |
|---|---|---|---|
| PEG-600 | 30 | 723 | 1.05 |
| PEG-1540 | 20 | 1560 | 1.08 |
| PEG-3000 | 12 | 3014 | 1.08 |
| PEG-4500 | 9 | 4467 | 1.08 |
| PEG-6000 | 6 | 5921 | 1.08 |
| PEG-18500 | 2 | 18 520 | 1.08 |
| PEODME−600 | 40 | 619 | 1.02 |
| PEODME−1000 | 30 | 1015 | 1.03 |
| PEODME−3000 | 12 | 2998 | 1.07 |
| PEODME−4300 | 8 | 4319 | 1.08 |
| PEODME−6000 | 5 | 5993 | 1.08 |

**Table 3. Acceptance Percentages (and Trial Ratios) of Selected Moves Used for the PEG-3000 and PEODME-3000 Systems at 450 K and 0.1 MPa**

| | rep | EB | DB | CBMC (4 units) | SAFE-CBMC (4 units) |
|---|---|---|---|---|---|
| PEODME | (20%) | (20%) | (20%) | (10%) | (0%) |
| | 1.5 | 0.08 | 0.0035 | 8.8 | 6.9 |
| PEG | (0%) | (30%) | (30%) | (10%) | (10%) |
| | N/A | 0.025 | 0.0031 | 4.0 | 6.3 |

for each system, are given in Table 2. The percentage of the move attempts for all systems, unless stated otherwise, and the acceptance percentages for these moves for the PEODME−3000 and PEG-3000 systems are given in Table 3. It should be noted that the reptation move was not used for the PEG system, because it required, in addition to the reptation of a repeat unit, the regrowth of both (O−H) end points, which was found to have a prohibitively low acceptance rate. Furthermore, the rotational and translational moves were both attempted with a frequency of 10%, and had their maximum displacements adjusted to result in an acceptance rate of 50%. Volume fluctuation moves were attempted at a frequency of 0.1%, and had their maximum displacement set to lead to a 10% acceptance rate. Unless noted otherwise, all simulations consisted of runs of 800 000 Monte Carlo (MC) cycles (one MC cycle is $N$ MC moves). All errors were taken by averaging between four runs of 200 000 MC cycles.

**End-Bridging.** For PEODME, the procedure for the EB move follows closely that used previously for the simulation of polymer chains, but instead of using geometric criteria for the chain bridging,[15] the SAFE-CBMC method is used.[38] The procedure used for an EB move going from state $\mathscr{A}$ to state $\mathscr{B}$ for PEODME is illustrated in Figure 1, and can be described as follows. (a) A chain end (α) of a random chain **B** is chosen at random, followed by the random determination of the number of beads to be regrown, ranging from 3 to 6 (3 in the illustration). (b) Multiple possible target atoms (*ntarget*) are tried, picking one ($\beta$) based on intramolecular bead−bead probability distribution functions which are updated throughout the simulation. (c) A growth is performed between α and the target atom, $\beta$, using the SAFE-CBMC method. (d) The procedure is repeated for the reverse move (from $\gamma$ to α) to ensure microscopic reversibility. (e) The move is accepted or rejected based on the acceptance probability below.

$$P(\mathrm{EB})_{\mathscr{A}\to\mathscr{B}} = \min\left[1, P_{\mathrm{SAFE-CBMC}} \times \frac{[\sum_{j=1}^{n_{\mathrm{target}}} P_j(r)]_{\mathscr{A}\to\mathscr{B}}}{[\sum_{j=1}^{n_{\mathrm{target}}} P_j(r)]_{\mathscr{B}\to\mathscr{A}}} \frac{[P_\alpha(r)]_{\mathscr{B}\to\mathscr{A}}}{[P_\beta(r)]_{\mathscr{A}\to\mathscr{B}}}\right] \quad (6)$$

$P_{\mathrm{SAFE-CBMC}}$ is the acceptance probability for the SAFE-CBMC regrowth, and $P_i(r)$ represent the intramolecular bead−bead distributions mentioned in step (b) between α and $\beta$ for the forward move, and between $\gamma$ and α for the reverse move. The criteria for the determination of these probability distributions can be found in ref 38.

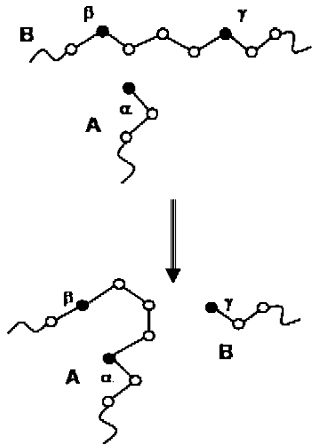


**Figure 1.** Schematic of the end-bridging move used in this work.

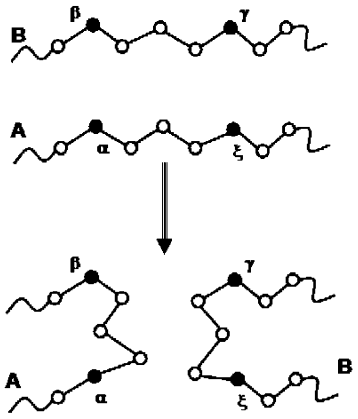


**Figure 2.** Schematic of the double-bridging move used in this work.

For the execution of an EB move for PEG, which is capped by alkanol groups, a slightly different approach has to be taken than with PEODME. During an EB move, the methyl group (α) of the chosen PEODME end point in step a can be simply changed into a methylene unit, and be followed by (a) SAFE-CBMC growth to connect with chain **B**. For PEG, though, the alpha methylene group is chosen in step (a) (not the end point as is the case with PEODME), followed by the elimination of the −OH end group, followed by the growth toward the target site, $\beta$, as with PEODME. To complete the move, though, the alkanol group has to be regrown from $\gamma$ using conventional CBMC. The movement of this hydrogen-bonding group to another position significantly decreases the acceptance probability for this move, but, as will be discussed below, can help in speeding up the equilibration of the polymer melt.

**Double-Bridging.** The DB move utilized is again similar to that used previously,[16] but instead of geometric criteria, uses SAFE-CBMC to bridge the two polymers. A similar modification to the DB move has been described in detail elsewhere,[39] and was used to successfully sample high molecular weight polyethylene melts. Furthermore, the polymer chains simulated in the present work are polydisperse, while those used previously were monodisperse.

The procedure for going from state $\mathscr{A}$ to state $\mathscr{B}$, illustrated in Figure 2, is the same for both PEG and PEODME, and can be described as follows. (a) A chain (**A**) and atom (α) are chosen at random, followed by the random determination of the number of sites to grow ranging from 3 to 6 (3 in Figure 2). (b) Multiple possible target atoms are tried, choosing one based on the $P(r)$ values for α to $\beta$, and also $\gamma$ to $\xi$. (c) A growth, using SAFE-CBMC is performed from α to $\beta$ followed by a SAFE-CBMC growth from $\gamma$ to $\xi$. (d) The procedure is repeated for the reverse move. (e) The move is accepted or rejected based on a similar acceptance probability, as given for the EB move

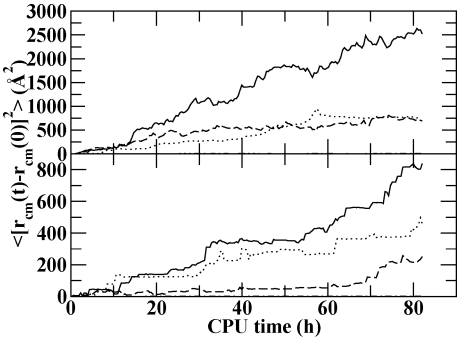


**Figure 3.** Translation of chain center of mass for PEODME-3000 (top) and PEG-3000 (bottom) as a function of computer time. Solid, dotted, dashed, and dot−dashed lines represent simulations using all moves, without EB, without DB, and without EB and DB moves, respectively.

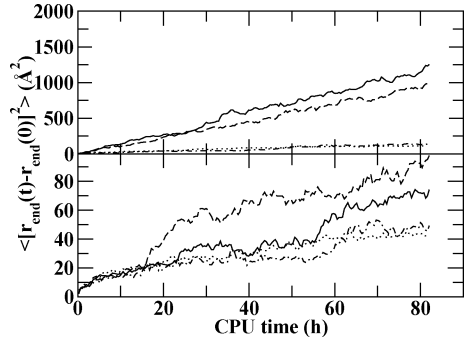


**Figure 4.** Translation of chain end-segments for PEODME-3000 methyl group (top) and PEG-3000 alkanol oxygen group (bottom) as a function of computer time. Lines represent the same as they do in Figure 3.

in eq 6. The only difference is that both $P_{\mathrm{SAFE-CBMC}}$ and $P_i(r)$ constitute products of the growth and distribution functions respectively for α to $\beta$ and $\gamma$ to $\xi$ for the forward move, and α to $\xi$ and $\gamma$ to $\beta$ for the reverse move.

## Results and Discussion

**Testing of Equilibration Methods.** Simulations were performed on the PEG-3000 and PEODME-3000 systems at a temperature of 450 K and a pressure of 0.1 MPa with total runs being 400 000 MC cycles. When a single bridging move was not used, the trial percentage of the other was doubled. For the case when neither of the bridging moves were used, the trial percentage of the CBMC and SAFE-CBMC moves were increased equally, leaving all other trial percentages fixed.

The displacements of the chain centers of mass are given in Figure 3. For the PEODME system, the center of mass displacement is not significantly affected by the type of bridging move used, but when neither EB nor DB moves are used, the displacement is greatly reduced, becoming barely noticeable on the plot (it reaches around 5 Å$^2$ at 80 h of CPU time), as has been shown before.[16,35] For the PEG system, though, the type of bridging move strongly affects the center of mass displacement. It can be clearly observed that the DB move is much more efficient at displacing the center of mass, and the simulations without the EB or DB moves show even a smaller center of mass displacement than for the similar case in the PEODME system (reaching 2.2 Å$^2$ at 80 h of CPU time). This is expected, since no reptation moves are used, and the acceptance rate of the CBMC moves is lower. The reason the type of bridging move has little effect on the PEODME system, but a strong effect on the PEG system, is that the acceptance rate of the EB move is much lower (by a factor of 3) in PEG than in PEODME, while the acceptance rate of the DB move is similar between the two polymers (Table 3).

The displacements of the chain end-segments (methyl for PEODME and oxygen for PEG) are given in Figure 4. The displacement of the end-segments is much faster for PEODME than for PEG in all cases. The differences between PEODME and PEG when not using connectivity-altering moves show that the use of the reptation move and the factor of 2 higher acceptance for the CBMC move (see Table 3) results in only a moderate increase in the mass transfer of the end-segments. While the acceptance rate of the EB move for PEODME is a factor of 3 higher than for PEG, the difference in end-segment displacement is too large to be accounted for by the difference in EB acceptance alone. Apparently, the combination of the reptation (which has an acceptance rate 20 times higher than the EB move) and the EB move for PEODME allows for a very rapid increase in the displacement of the polymer end-segments. One of the possible reasons for this is that "shuttling", i.e. the situation wherein following an accepted EB move from state $\mathscr{A}$ to state $\mathscr{B}$ (see Figure 1), the reverse move ($\mathscr{B}$ to $\mathscr{A}$) tends to be accepted soon thereafter, can be avoided by an acceptance of a reptation move between the EB moves. Since there is no reptation move for PEG, shuttling can seriously hamper the end-segment displacement. Nevertheless, the use of EB still results in a factor of 2 increase in the end-segment displacement (four in the squared displacement) of PEG, compared to when it is not used.

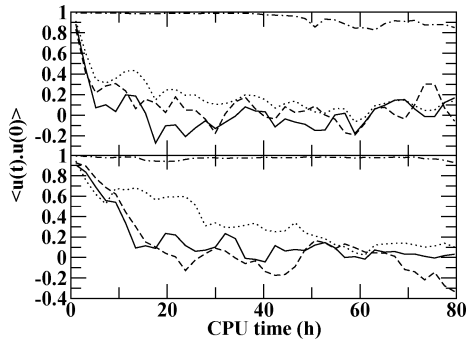


**Figure 5.** Decay of end-to-end autocorrelation function for PEODME-3000 (top) and PEG-3000 (bottom) as a function of computer time. Lines represent the same as they do in Figure 3.

The decay of the autocorrelation function of the end-to-end vector as a function of computer time is shown in Figure 5, showing that for these systems, both bridging moves have similar performance in the decay of the vector. It is interesting to note that the DB move appears to do a slightly worse job at equilibrating the end-to-end vector than the EB move for PEO polymers with a molecular weight of around 6000. The lower acceptance of the DB move is likely the main reason for this. Also, it appears that the autocorrelation function decays somewhat more rapidly for the PEODME system than for the PEG system, following a pattern similar to that observed for the chain end-segment and center of mass displacements. An overall conclusion is that, in general, PEODME is significantly easier to equilibrate with our MC moves than PEG, and that the connectivity-altering moves significantly increase both

**Table 4. Densities of Polymer Melts**

| | | | density (g/cm$^3$) | |
|---|---|---|---|---|
| | $T$ (K) | $p$ (MPa) | sim | exp |
| PEG-600 | 383.25 | 0.1 | $1.061_2$ | 1.059 |
| PEG-600 | 471.75 | 0.1 | $0.990_2$ | 0.990 |
| PEG-600 | 471.75 | 100.0 | $1.061_4$ | 1.055 |
| PEG-1540 | 474.65 | 0.1 | $0.966_5$ | 0.977 |
| PEG-18500 | 471.75 | 0.1 | $0.988_2$ | 0.990 |
| PEOMME−750 | 325.25 | 0.1 | $1.086_2$ | 1.083 |
| PEODME−600 | 343.35 | 0.1 | $1.042_2$ | 1.034 |
| PEODME−600 | 303.05 | 0.1 | $1.064_2$ | 1.067 |
| PEODME−600 | 303.05 | 100.0 | $1.111_1$ | 1.111 |
| PEODME−1000 | 343.35 | 0.1 | $1.063_8$ | 1.051 |

[a] The subscripts represent the uncertainties in the last digit(s).

**Table 5. Conformational Populations at $T$ = 343 K**

| | C−C−O bond pair | | | | |
|---|---|---|---|---|---|
| | *gt* | $g^{\pm}g^{\mp}$ | *tt* | *tg* | $g^{\pm}g^{\pm}$ |
| Smith et al.[a] | 0.540 | 0.134 | 0.188 | 0.063 | 0.075 |
| this work | 0.548 | 0.118 | 0.175 | 0.068 | 0.091 |

| | C−O−C bond pair | | | |
|---|---|---|---|---|
| | *tt* | *tg* + *gt* | $g^{\pm}g^{\mp}$ | $g^{\pm}g^{\pm}$ |
| Smith et al.[a] | 0.505 | 0.441 | 0.014 | 0.040 |
| this work | 0.496 | 0.465 | 0.003 | 0.036 |

[a] Interpolated data between temperatures 343 and 373 K taken from ref 40.

the mass transfer of the polymer and its long range conformational equilibration.

**Densities.** Comparisons between experimental and simulated mass densities are given in Table 4. The agreement between the two sets is excellent, especially considering the simplicity of the models (being united atom and LJ plus point charge potentials), and the fact that the potential parameters were fit to small ether, alkanol, and glycol molecules.[28,29] Most simulated values are well within 1% of experiment, while for two cases the discrepancy is 1.1%. This shows that the TraPPE force field is rigorous over a moderate range of temperature, and a very large range of molecular weight for both PEG and PEODME. More striking is the fact that the model correctly predicts densities over a very large range of pressures as well, despite the fact that a LJ potential is used. The LJ potential has a pairwise atomic repulsion of $(\sigma/r)$,[12] which is sharper than the quantum mechanically derived exponential atomic repulsion.

**Torsional Populations.** The pairwise torsional populations of the TraPPE force field compared with those of Smith et al.[40] are given in Table 5. The gauche states for the dihedral angles are defined such that $60° \leq g^+ < 180° \leq g^- < 300°$, and the trans conformations are considered when dihedral angles are outside of that range. The results were taken from a melt of PEODME−600 chains at a temperatures of 343 K and a pressure of 0.1 MPa. A close similarity between the two force fields is seen for the torsional populations. This is expected, since the O−C−C−O torsional potential used in this work was fit to the one used by Smith et al.,[22] and the only difference is in the C−C−O−C potential, which in this work was taken from the OPLS force field,[30] but the overall agreement between the torsional populations is shown to be quite good.

**Structure Factor.** The static structure factor is defined as follows:

$$S(q) = 1 + \frac{1}{\langle V \rangle} \frac{\sum_{\alpha,\beta} N_\alpha N_\beta b_\alpha b_\beta \int [g_{\alpha,\beta}(r) - 1] e^{-i\mathbf{q}\cdot\mathbf{r}} d^3r}{\sum_\alpha N_\alpha {b_\alpha}^2} \quad (7)$$

where $\langle V \rangle$ is the average volume, $N_\alpha$ and $b_\alpha$ are the total number and coherent scattering length, respectively, for sites of type α, and $g_{\alpha,\beta}(r)$ is the pairwise radial distribution function (RDF) between sites of type α and $\beta$.

For the determination of the structure factor, 100 000 MC cycles of a PEODME-3000 melt were simulated at a temperature of 363 K and a pressure of 1 atm, in accordance with the experimental conditions on a deuterated PEO melt with a weight-averaged molecular weight of $M_w$ = 23.2 kg/mol.[41] Artificial deuterium atoms were added a posteriori to the MC configurations at a bond length of 1.1 Å from the methyl and methylene pseudo-atom positions, using bond angles of: D−C−D = 108°, and O−C−D and C−C−D = 109.5°.

The static structure factor for neutron diffraction obtained from the MC simulations is given in Figure 6 along with an experimental structure factor.[41] The result shows an overall good agreement between simulation and experiment for the structure factor. The MC simulation results show a slightly more ordered structure factor overall, which could be due to the absence of hydrogens, or any vibrations in the MC simulations (bond lengths are kept fixed). In addition, the large peak at 1.4 Å$^{-1}$ is higher for the MC simulations, indicating a slight overestimation of intermolecular ordering between the chains.

**Radii of Gyration and End-to-End Distances.** The mean squared end-to-end distances $\langle R^2 \rangle$ and radii of gyration $\langle {R_g}^2 \rangle$ as functions of chain length have been calculated for both PEG and PEODME up to molar masses of 6000 g/mol at a temperature of 450 K. The results for the $\langle R^2 \rangle$ distances and six times the $\langle {R_g}^2 \rangle$ values as functions of the number of backbone atoms are given in Figure 7 with linear fits applied to them. Because of the fact that polydisperse samples are used in these simulations, each individual simulation provides data for many different chain lengths. After gathering average values for each chain length and calculating the error of the mean, we perfomed a weighted fit on each value to narrow their number to around three per system. The results show moderately different behavior between the PEODME and PEG systems, and nearly identical behavior between curves calculated using the $\langle R^2 \rangle$ and $\langle {R_g}^2 \rangle$ values. The slopes of the linear fits gave the following relations for the $\langle R^2 \rangle$ and the $\langle {R_g}^2 \rangle$ values for PEODME.

$$\langle R^2 \rangle = 0.793M \text{ (Å}^2\text{)}$$

$$\langle {R_g}^2 \rangle^{1/2} = 0.364M^{1/2} \text{ (Å)}$$

It is often assumed that $\langle R^2 \rangle = 6\langle {R_g}^2 \rangle$, and in this case, they are practically equal as a function of molecular weight. In addition, if compared with the results of SANS experiments,[40] which give a $\langle {R_g}^2 \rangle^{1/2} = 119.5$ Å for a PEG melt with $M = 110$ kg/mol at 459 K, extrapolating the simulation results using the linear fit gives a value of 120.6 Å, showing excellent agreement.

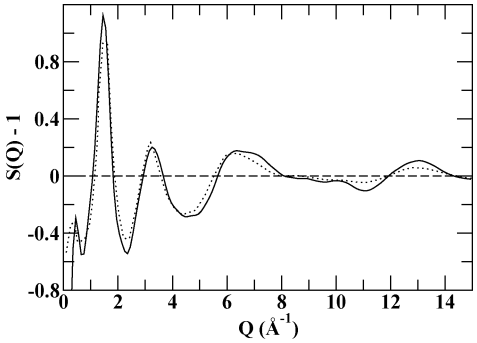


**Figure 6.** Static structure factor for deuterated PEO with the solid line being simulation, and dotted line being experiment.[40]

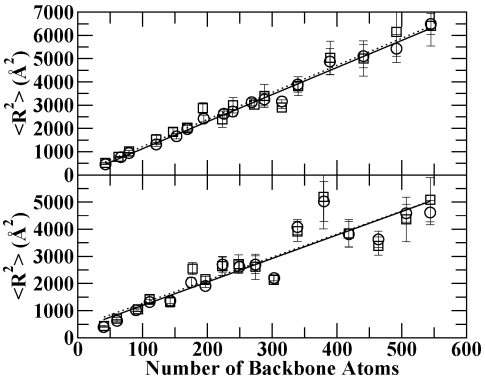


**Figure 7.** Six times the mean squared radius of gyration (circles, solid lines) and the mean squared end-to-end length (squares, dotted lines) as a function of chain length with linear fits applied to them (lines) for PEODME (top) and PEG (bottom).

MC simulations for PEG gave the following values:

$$\langle R^2 \rangle = 0.590M \text{ (Å}^2\text{)}$$

$$\langle R_g{}^2 \rangle^{1/2} = 0.311M^{1/2} \text{ (Å)}$$

The values for PEG are significantly lower than those for PEODME, and do not agree well with experimental data as the PEODME results do. At first glance, this may seem troubling, since the experimental data being compared with were derived from a PEG polymer, but the molecular weight of that polymer was very high at 110 kg/mol.[40] Because of the strong end group effects for the PEG samples, it would be expected for the polymer to behave differently at lower molecular weights, while at higher molecular weights, end group contributions to the polymer structure would be negligible. It can also be observed that there is a larger spread in values for high molecular weights for the PEG system compared with PEODME. This is likely due to the higher difficulty in sampling the PEG chains.

After the compilation of the end-to-end distance, the characteristic ratio can be estimated as follows.

$$C_{X-1} = \frac{\langle R^2 \rangle}{(X-1)\bar{l}^2} \tag{8}$$

where $X - 1$ is the number of bonds in the chain backbone, and $\bar{l}^2$ is the average squared skeletal bond length of 2.135 Å$^2$. As previously, $6\langle R_g{}^2 \rangle$ can be used in place of $\langle R^2 \rangle$. Figure 8 gives the characteristic ratio calculated using both the $\langle R^2 \rangle$ and the $\langle R_g{}^2 \rangle$ values for PEODME and PEG. In general, it is expected that

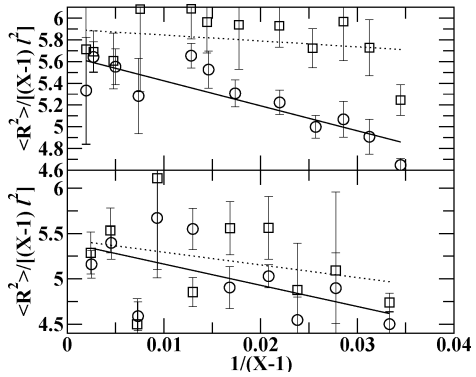


**Figure 8.** Characteristic ratio plots obtained from both end-to-end distances and radii of gyration, along with their linear fits. Symbols and positions are the same as in Figure 7.

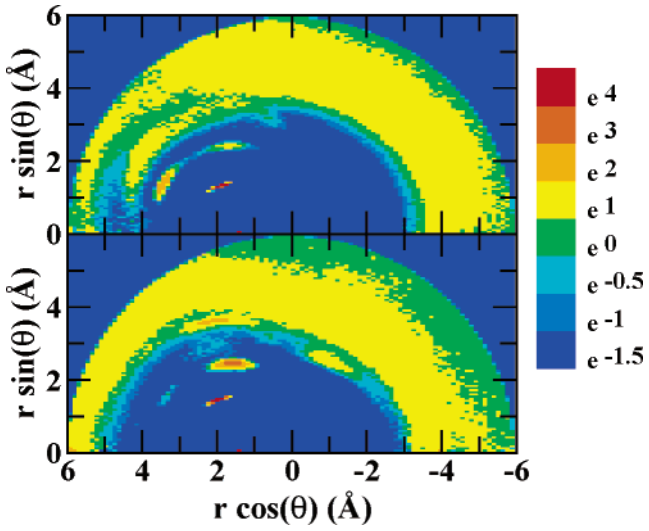


**Figure 9.** Three-dimensional radial-angular distribution functions, in polar coordinates, between oxygen end groups of PEG and all other heavy atoms (bottom) and between methyl end groups of PEODME and all other heavy atoms (top).

characteristic ratios extracted from $\langle R^2 \rangle$ and from $\langle R_g{}^2 \rangle$ may be different for short chains; they should converge in the limit of very long chains. This behavior is observed in our simulations of both PEODME and PEG. Extrapolating the values to $1/(X - 1) = 0$ will give $C_\infty$. For PEODME, the $C_\infty$ values calculated from the end-to-end distances and the radii of gyration are 5.6 and 5.9, respectively. These are relatively close, despite the clear differences in the slopes of the linear fits. This result compares favorably with the SANS experiments[40] of PEG at 459 K of 5.5. The values for PEG calculated using the end-to-end distances and radii of gyration are both 5.4, slightly lower than values calculated for PEODME, but still in good agreement with the SANS experiments.

**Distribution Functions.** Distribution functions were calculated from 100 000 MC cycles of simulations of both PEODME−600 and PEG-600 at a temperature and pressure of 363 K and 1 atm, respectively. The radial-angular distribution functions ($g(r,\theta)$), in polar coordinates, between the end groups (methyl for PEODME and oxygen for PEG), and all other heavy atoms, including those bonded to the end groups, are given in Figure 9. The cutoff for the function was chosen to be 6 Å to magnify the first solvation shell. The $g(r,\theta)$ function is similar to a radial distribution function in that it represents the probability to find another atom as a

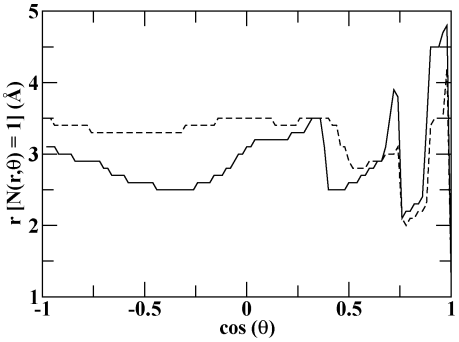


**Figure 10.** Radial and angular position in which the integral of the radial-angular distribution functions given in Figure 9 is one for PEG (solid line) and PEODME (dashed line).

function of $r$, normalized by the uniform density of the system, but adds an angular dimension of $\theta$. Values for $\theta$ are determined by calculating an angle between the vector connecting the end group atom (methyl for PEODME and oxygen for PEG) with the preceding atom in the chain (oxygen for PEODME and methylene for PEG), and the vectors connecting the end group atom to all remaining heavy atoms. For example, the reader can observe at $r \sin(\theta) = 0$ and $r \cos(\theta) = 1.4$ Å a single point in the diagram representing the penultimate pseudo-atom in the chain (methylene for PEG, and oxygen for PEODME). In addition, PEG displays a peak at $r \cos(\theta) = -1$ Å and $r \sin(\theta) = 2.5$ Å, which represents a hydrogen bond with another ether or alkanol oxygen. While the O−H- -O angle is zero, the $CH_2$−O- -O angle is 108.5°, and the first peak in the oxygen−oxygen radial distribution function is at $r \approx 3$ Å. It can be observed that this peak appears for PEG, and not for PEODME. Focusing on the intramolecular correlations, there is a strong peak for both systems at $r \cos(\theta) = 2$ Å and $r \sin(\theta) = 1.2$ Å representing the pseudo-atom located two bonds away. In addition, nearby this peak are two additional peaks representing the pseudo-atom that is three bonds away. It is clear that, while PEODME has two strong peaks representing the gauche and trans states, with the trans being moderately higher, PEG only has one strong peak representing the gauche state, with the trans state having a very weak peak in comparison. This is due to the intramolecular hydrogen bond that the hydrogen in PEG forms with its first ether oxygen.

Taking the integral of a standard radial distribution function, without its normalizations, can give the average number of atoms within a certain distance of a chosen atom. The same can be done for $g(r,\theta)$ over $r$ at constant $\theta$. The positions where the $g(r,\theta)$ functions integrated by this method for the PEODME and PEG end groups reach unity are given in Figure 10. These represent the distances (as a function of $\theta$) at which an end group atom would most likely see another heavy atom, and thus constitute a good basis for determining the excluded volume as a function of $\theta$ for the two end groups. It can be observed that hydrogen bonding results in a wide range of excluded molar volumes for PEG between $\cos(\theta) = -1.0$ and $\cos(\theta) = 0.3$. Over the same region, the corresponding excluded volumes for the end groups of PEODME are pretty flat and at a higher value. In addition, the regions near $\cos(\theta) = 0.5$ for both PEG and PEODME show the smaller molar volume of PEG is due to intramolecular hydrogen bonding with the first ether oxygen. For PEG, though, there is a significantly higher excluded volume above $\cos(\theta) = 0.65$ compared with PEODME. Much of this can be attributed to the large differences in excluded volume in areas just outside the depression around $\cos(\theta) = 0.8$. This is because of the higher and broader peak in Figure 9 of the trans state representing the dihedral formed by the pseudo-atom separated by three bonds from the end group atom for PEODME compared with PEG. In this region, intramolecular correlations of the end group are stronger and more directed in the case of PEG, leading to a higher excluded volume at nearby angles.

Integrating out the curves shown in Figure 10 would give the total excluded volume for each group. The total excluded volumes, calculated in this way, for the PEODME and PEG end groups are 162 and 127 Å$^3$, respectively. The excluded volume for the PEODME methyl end groups is significantly higher than that for the PEG oxygen end groups. This lends to the notion that the differences in the molecular weight dependence of volumetric properties between PEG and PEODME is strongly affected by the difference in the end groups' excluded volume, which is in agreement with the conclusions of ref 18. It has been argued that the difference in end group excluded volume is due to differences in the number of degrees of freedom.[18] Observing Figure 9, the alkanol end group of PEG is moderately restricted to be in either the intermolecular ($r \cos(\theta) = -1$ Å and $r \sin(\theta) = 2.5$ Å), or intramolecular ($r \cos(\theta) = 1.5$ Å and $r \sin(\theta) = 2.5$ Å) hydrogen bonding positions, while the range of motion of the methyl end group of PEODME appears to be much broader at these positions. The largest decrease in excluded volume of the alkanol end group in comparison to the methyl one, however, can clearly be observed to result from its closer proximity to the species to which it is hydrogen-bonded intermolecularly (Figure 9); it is not directly related to differences in degrees of freedom. While both effects may play an important role in affecting volumetric properties, the dominant one, which is mainly responsible for observed differences in excluded volume, appears to be the stronger tendency for attraction of the alkanol group to its first intermolecular neighbors (other oxygen atoms), and consequent smaller distance from these neighbors.

## Conclusions

Connectivity-altering Monte Carlo simulations using the TraPPE-UA force field for poly(ethylene oxide) end-capped with methyl (PEODME) and glycol (PEG) groups were performed for a variety of temperatures, pressures, and molecular weights. The combination of end-bridging and double-bridging moves, using SAFE-CBMC for the bridging, was shown to do a good job in equilibrating polymer melts of moderate to high molecular weights. Also, the TraPPE-UA force field proved to be successful in reproducing liquid densities, packing and chain conformations over a wide range of physical conditions. Differences in the molecular weight dependence of the volumetric properties were linked to the different excluded volumes of the end-segments. Microscopically, it can be seen that the intermolecular hydrogen bonding tendency of the hydroxy end group causes it to be closer to oxygen atoms than the methyl group in PEODME is to any atom with which it is not directly bonded.

**Acknowledgment.** The authors are grateful to the National Science Foundation for the award of an NSF-

MPS Distinguished International Postdoctoral Fellowship to C.D.W.

## References and Notes


(1) Cappello, B.; Del Nobile, M. A.; La Rotonda, M. I.; Mensitieri, G.; Miro, A.; Nicolais, L. *Parmaco* **1994**, *49*, 809.
(2) Jeon, S. I.; Lee, J. H.; Andrade, J. D.; de Gennes, P. G. *J. Colloid Interface Sci.* **1991**, *142*, 129.
(3) O'Neill, M. L.; Cao, Q.; Fang, M.; Johnston, K. P.; Wilkinson, S. P.; Smith, C. D.; Kerschner, J. L.; Jureller, S. H. *Ind. Eng. Chem. Res.* **1998**, *37*, 3067.
(4) Drohmann, C.; Beckman, E. J. *J. Supercrit. Fluids* **2002**, *22*, 103.
(5) Gray, F. M. *Polymer Electrolytes;* The Royal Society of Chemistry: Cambridge, U.K., 1997.
(6) Bruce, P. G.; Vincent, C. A. *J. Chem. Soc., Faraday Trans.* **1993**, *89*, 3187.
(7) Croce, F.; Appetecchi, G. B.; Persi, L. Scrosati, B. *Nature (London)* **1998**, *394*, 456.
(8) Ding, J. Maitra, P.; Wunder, S. L. *J. Polym. Sci.* **2003**, *41*, 1978.
(9) Johnson, J. A.; Sabourngi, M. L. Price, D. L.; Ansell, S. *J. Chem. Phys.* **1998**, *109*, 7005.
(10) Borodin, O.; Douglas, R.; Smith G. D.; Trouw, F.; Petrucci, S. *J. Phys. Chem. B* **2003**, *107*, 6813.
(11) Lin, B.; Boinske, P. T.; Halley, J. W. *J. Chem. Phys.* **1996**, *105*, 1668.
(12) Müller-Plathe, F. *Acta Polym.* **1994**, *45*, 259.
(13) Sasanauma, Y.; Ohta, H.; Touma, I.; Matoba, H.; Hayashi, Y.; Kaito, A. *Macromolecules* **2002**, *35*, 3748.
(14) Auhl, R.; Everaers, R.; Grest, G. S.; Kremer, K.; Plimpton, S. J. *J. Chem. Phys.* **2003**, *119*, 12718.
(15) Pant, P. V. K.; Theodorou, D. N. *Macromolecules* **1995**, *28*, 7224.
(16) Karayiannis, N. C.; Mavrantzas, V. G.; Theodorou, D. N. *Phys. Rev. Lett.* **2002**, *88*, 105503.
(17) Theodorou, D. N. in Nielaba, P.; Mareschal, M.; Ciccotti, G. (Eds.) *Bridging Time Scales: Molecular Simulations for the Next Decade* Springer-Verlag: Berlin, 2002; p 67.
(18) Dee, G. T.; Ougizawa, T.; Walsh, D. J. *Polymer* **1992**, *33*, 3462.
(19) Zoller, P.; Walsh, D. J. *Standard Pressure−Volume−Temperature Data for Polymers*; Technomic Publishing Company: Lancaster, PA, 1995.
(20) Flory, P. J.; Orwoll, R. A.; Vrij, A. *J. Am. Chem. Soc.* **1964**, *86*, 3507.
(21) Lennard-Jones, J. E.; Devonshire, A. F. *Proc. R. Soc. London, A* **1937**, *163*, 53.
(22) Smith, G. D.; Jaffe, R. L.; Yoon, D. Y. *J. Phys. Chem.* **1993**, *97*, 12752.
(23) Borodin, O.; Smith, G. D. *J. Phys. Chem. B* **2003**, *107*, 6801.
(24) Rigby, D.; Sun, H.; Eichinger, B. E. *Polym. Int.* **1997**, *4*, 880.
(25) Martin, M. G.; Siepmann, J. I. *J. Phys. Chem. B* **1998**, *102*, 2569.
(26) Martin, M. G.; Siepmann, J. I. *J. Phys. Chem. B* **1999**, *103*, 4508.
(27) Wick, C. D.; Martin, M. G.; Siepmann, J. I. *J. Phys. Chem. B* **2000**, *104*, 8008.
(28) Chen, B.; Potoff, J. J.; Siepmann, J. I. *J. Phys. Chem. B* **2001**, *105*, 3093.
(29) Stubbs, J. M.; Potoff, J. J.; Siepmann, J. I. *J. Phys. Chem. B*, submitted for publication.
(30) Jorgensen, W. L.; Madura, J. D.; Swenson, C. J. *J. Am. Chem. Soc.* **1984**, *106*, 813.
(31) Lorentz, H. A. *Ann. Phys.* **1881**, *12*, 127.
(32) Berthelot, D. *C. R. Hebd. Seances Acad Sci.* **1889**,*126*, 127.
(33) Mavrantzas, V. G.; Boone, T. D.; Zervopoulou, E.; Theodorou, D. N. *Macromolecules* **1999**, *32*, 5072.
(34) Doxastakis, M.; Mavrantzas, V. G.; Theodorou, D. N. *J. Chem. Phys.* **2001**, *115*, 11339.
(35) Gestoso, P.; Nicol, E.; Doxastakis, M.; Theodorou, D. N. *Macromolecules* **2003**, *36*, 6925.
(36) Siepmann, J. I. *Mol. Phys.* **1990**, *70*, 1145.
(37) de Pablo, J. J. Laso, M.; Suter, U. W. *J. Chem. Phys.* **1992**, *96*, 2395.
(38) Wick, C. D.; Siepmann, J. I. *Macromolecules*, **2000**, *33*, 7207.
(39) Banaszak B. J.; de Pablo J. J. *J. Chem. Phys.* **2003**, *4*, 2456.
(40) Smith, G. D.; Yoon, D. Y.; Jaffe, R. L.; Colby, R. H.; Krishnamoorti, R.; Fetters, L. J. *Macromolecules* **1996**, *29*, 3462.
(41) Annis, B. K.; Borodin, O.; Smith, G. D.; Benmore, C. J.; Soper, A. K.; Londono, J. D. *J. Chem. Phys.* **2001**, *115*, 10998.


MA049193R